J. Fluid Mech. (2003), *vol.* 480, *pp.* 95–118.
DOI: 10.1017/S0022112002003531 Printed in the United Kingdom

Rheology of suspensions with high particle inertia and moderate fluid inertia

By JONATHAN J. WYLIE[1], DONALD L. KOCH[2] AND ANTHONY J. C. LADD[3]

[1]Department of Mathematics, City University of Hong Kong, Tat Chee Avenue, Kowloon, Hong Kong

[2]Department of Chemical Engineering, Cornell University, Ithaca, NY 14853, USA

[3]Department of Chemical Engineering,University of Florida, Gainesville, FL 32611, USA

(Received 17 August 2001 and in revised form 23 July 2002)

We consider the averaged flow properties of a suspension in which the Reynolds number based on the particle diameter is finite so that the inertia of the fluid phase is important. When the inertia of the particles is sufficiently large, their trajectories, between successive particle collisions, are only weakly affected by the interstitial fluid. If the particle collisions are nearly elastic the particle velocity distribution is close to an isotropic Maxwellian. The rheological properties of the suspension can then be determined using kinetic theory, provided that one knows the granular temperature (energy contained in the particle velocity fluctuations). This energy results from a balance of the shear work with the loss due to the viscous dissipation in the interstitial fluid and the dissipation due to inelastic collisions. We use lattice-Boltzmann simulations to calculate the viscous dissipation as a function of particle volume fraction and Reynolds number (based on the particle diameter and granular temperature). The Reynolds stress induced in the interstitial fluid by the random motion of the particles is also determined. We also consider the case where the interstitial fluid is moving relative to the particles, as would occur if the particles experienced an external body force. Owing to the nonlinearity of the equations of motion for the interstitial fluid, there is a coupling between the viscous dissipation caused by the fluctuating motion of the particles and the drag associated with a mean relative motion of the two phases, and this coupling is explored by computing the dissipation and mean drag for a range of values of the Reynolds numbers based on the mean relative velocity and the granular temperature.

1. Introduction

Suspensions of solid particles in a liquid or gas are important and widespread in many industrial and geophysical applications. Examples include fluidized beds, sediment transport, and slurry flows. In order to make progress with these problems, a fundamental understanding of the underlying dynamics is essential. Suspension flows typically involve huge numbers of particles with a wide difference between the scale of the particles and the scale of the flow. In addition the dynamically complicated fluid–particle interactions implicit in such flows make direct computer simulation of large-scale suspension flows far beyond the capabilities of even the fastest computers. Therefore, we take the approach of developing a set of continuum equations for the bulk flow that incorporates the complex particle-scale dynamics. Since relatively small computer simulations can be used to determine the dynamics of the

suspension at the particle level we can therefore determine the appropriate continuum equations.

Kinetic theories for suspensions in which the particle inertia is large can be formulated based on analogy to the kinetic theory of dense gases, provided that one has a means of computing the dissipation of energy. However, currently available theories are restricted to situations where the continuous phase is unimportant (Lun *et al.* 1984) or the suspending gas has no inertia (Sangani *et al.* 1996). In many applications the Reynolds number (based on the particle diameter) is sufficiently large that the effects of fluid inertia must be considered. We will determine the rate of viscous dissipation of the kinetic energy in the particle phase and the mean drag force acting on an array of particles with a Maxwellian velocity distribution. This will allow the above-mentioned kinetic theories to be extended to the more general situation where the continuous phase is a finite-Reynolds-number gas or liquid.

Despite the prevalence and importance of fluid inertia, relatively little is known about the average flow properties of such suspensions. Koch & Hill (2001) review the current state of knowledge and the challenges involved in modelling inertial suspensions. Many of the computational studies of finite-Reynolds-number particles have focused on the trajectories of individual particles or particle pairs (see, for example, Aidun, Lu & Ding 1998 and Qi 1999). Theoretical approaches modelling the behaviour of inter-penetrating continua (Drew & Passman 1999) provide a framework for understanding inertial multiphase flow but require the specification of semi-empirical constitutive equations. Recent work by Bunner & Tryggvasan (1999) shows that computational fluid mechanics is now capable of simulating the average behaviour of a suspension of many interacting three-dimensional particles at finite Reynolds number. However, computer simulation alone will not provide averaged equations of motion that can be used to predict a wide range of suspension behaviours. As stated above, the goal of our study is to combine computer simulations with kinetic theory to derive equations of motion for concentrated, inertial suspensions.

If the suspension is sufficiently energetic, then, between successive collisions, the particle trajectories will be only weakly affected by the presence of the fluid. If, in addition, the particle collisions are sufficiently close to elastic then the particle motions will be similar to those of molecules in a kinetic gas. Using similar ideas, detailed theories and appropriate continuum equations have been developed for rapid granular flow in which the inertia and inelasticity of the particles are important and the interstitial fluid is neglected (e.g. Lun *et al.* 1984; Jenkins & Richman 1988). These theories are based on Enskog's kinetic theory for dense gases, and assume the stress is due to the transport of momentum by random particle motions (kinetic stress) and instantaneous interparticle collisions (collisional stress). The energy contained in the random particle motions is controlled by a balance between the shear work and the energy loss due to inelastic interparticle collisions. In order to ensure that fluid mechanical effects are negligible, typical flow parameters require that the particles should be large, i.e. of the order of 1 mm in diameter, and that they should be suspended in a gas rather than a liquid. However, it is then difficult to ensure that the particles will remain suspended rather than collapsing due to gravity and undergoing enduring contacts. This limits the range of applicability of theories for rapid granular flow. In practice, experiments on granular flow are often done with particles in liquids (Bagnold 1956; Haines & Inman 1985) and the role of the interstitial fluid must be carefully examined.

Sangani *et al.* (1996) and Koch & Sangani (1999) have developed theories for sheared and sedimenting gas–particle flows, in which the Stokes number is large and

the particle Reynolds number is small. In this case, the particles have sufficient inertia to fly with relatively little change of velocity between successive interparticle collisions and the particulate phase can again be treated using kinetic theory. However, the viscous dissipation and mean drag force due to the interstitial gas are important in determining the rate of energy dissipation. The detailed gas flow among the particles is computed using a modified-multipole method (Sangani *et al.* 1996) for solving Stokes equations of motion for viscous-dominated flow. These theories are limited to gas–solid suspensions where the particle-to-fluid density ratio is large so that the dual limits of high Stokes number and low Reynolds number are simultaneously accessible. However, the drag on the particles grows with increasing Reynolds number and so the interstitial fluid will have the largest effect when the Reynolds number is moderately large. Furthermore, adhesive forces may become significant if the particles are small enough to have an asymptotically low Reynolds number flow. In this paper, we will extend these theories to finite Reynolds number so as to consider the behaviour of particle–gas suspensions with particle radii of order 50–500 μm diameter and particle–liquid suspensions with moderately large density ratios.

The principal aim of this paper is to obtain a basic understanding of the rheology of large-Stokes-number suspensions in which fluid inertia plays an important role. We consider suspensions subject to shearing motions that produce random particle velocity fluctuations in a manner similar to rapid granular flow. The energy balance for this fluctuation energy includes the viscous dissipation due to the interstitial fluid. We compute this dissipation using the lattice-Boltzmann method to determine the fluid velocity field among a random suspension of particles with a Maxwellian velocity distribution. The dissipation is determined over a wide range of particle concentrations as a function of a Reynolds number based on the root-mean-square particle velocity and particle diameter. To extend the theory to situations where there is a mean relative motion between the phases, we also determine the viscous dissipation of fluctuation energy in the presence of a mean relative motion, and the mean drag in the presence of fluctuating motion. The nonlinearity of the Navier–Stokes equations leads to a coupling between the forces associated with the fluctuating and mean motions. Hill, Koch & Ladd (2001 *a*, *b*) have presented an exhaustive study of the drag on particles in a fixed bed over a range of particle volume fractions and Reynolds numbers. Based on the results of Hill *et al.* for fixed beds, we present a simple theory to interpret the drag and dissipation in high-Stokes-number suspensions.

In general, the stress in a suspension consists of a viscous stress due to the mean shear, the viscous force-dipoles acting on the particles, the Reynolds stress of the fluid and the kinetic and collisional stresses of the particles (Batchelor 1970). As in the theories for gas–solid suspensions, we can neglect the viscous force dipoles due to the large Stokes number of the suspension. However, we compute the Reynolds stress associated with fluid motion induced by the random particle motions as well as considering the kinetic and collisional stresses of the particles.

2. Formulation

Results for granular materials (Lun *et al.* 1984) and low-Reynolds-number gas–solid suspensions (Sangani *et al.* 1996) have shown that flowing materials often have an internal structure that is close to a hard-sphere distribution with an isotropic Maxwellian distribution of particle velocities. This is true provided that the mechanisms that dissipate the kinetic energy of the particles have a weak effect on the particle trajectories. For granular materials, this corresponds to the case of

nearly elastic collisions between particles (a coefficient of restitution that is close to one), while for flowing suspensions there is an additional restriction based on the rate of viscous dissipation that will be discussed below. For small deviations from the Maxwellian distribution, Newtonian constitutive equations derived from kinetic theory can be invoked for the particulate phase. For larger deviations from isotropy, additional moments of the velocity distribution can be included to obtain normal stress differences that agree with the results of particle-dynamic simulations (Sangani *et al.* 1996).

The most important role of the fluid in a sheared suspension with large particle inertia is to dissipate the fluctuation energy. Thus, we examine an isotropic suspension of spherical particles in a viscous fluid or gas. We consider the case where the velocities of the particles are distributed over an isotropic Maxwellian distribution with variance given by

$$\langle (\boldsymbol{U} - \langle \boldsymbol{U} \rangle) \cdot (\boldsymbol{U} - \langle \boldsymbol{U} \rangle) \rangle = 3T, \tag{1}$$

where $\boldsymbol{U}$ is the velocity of an individual particle, angular brackets represent the average over all the particles in the suspension, and T is the granular temperature of the particles.

The volume fraction, defined as the volume of space occupied by solid particles, is

$$\phi = \tfrac{4}{3} n \pi a^3, \tag{2}$$

where n is the number of particles per unit volume and a is the particle radius. The Reynolds number, based on the granular temperature and the particle diameter, which represents the ratio between viscous and inertial forces on the particle scale, is

$$Re_T = \frac{2a\rho_f T^{1/2}}{\mu}, \tag{3}$$

where μ is the dynamic viscosity of the fluid and ρ_f is the mass density of the fluid. We define the Stokes number, which represents the ratio of the particle momentum to the momentum decrease due to Stokes drag as the particle translates through a distance equal to its radius, as

$$St = \frac{m T^{1/2}}{6\pi\mu a^2}, \tag{4}$$

where m is the particle mass. It should be noted that the Reynolds number and Stokes number are related by

$$St = \left(\frac{\rho_p}{\rho_f} \right) \frac{Re_T}{9}, \tag{5}$$

where ρ_p is the mass density of the individual particles.

The fluid phase is governed by the incompressible Navier–Stokes equations

$$\rho \left[\frac{\partial \boldsymbol{u}}{\partial t} + \boldsymbol{u} \cdot \nabla \boldsymbol{u} \right] = -\nabla p + \mu \nabla^2 \boldsymbol{u}, \tag{6}$$

$$\nabla \cdot \boldsymbol{u} = 0, \tag{7}$$

where $\boldsymbol{u}$ is the fluid velocity, t is time and p is the fluid pressure. The particulate and fluid phase are coupled by a no-slip boundary condition on the particle surfaces. The motion of the particles is governed by Newton's equations

$$m \frac{\mathrm{d}\boldsymbol{U}_i}{\mathrm{d}t} = \boldsymbol{F}_i, \tag{8}$$

$$\frac{2ma^2}{5}\frac{\mathrm{d}\boldsymbol{\Omega}_i}{\mathrm{d}t} = \mathscr{L}_i, \tag{9}$$

where $\boldsymbol{U}_i$ is the translational velocity and $\boldsymbol{\Omega}_i$ is the rotational velocity of the ith particle. $\boldsymbol{F}_i$ and $\mathscr{L}_i$ are the net force and torque on the ith particle, and include fluid stress, interparticle forces and external forces.

When two particles come sufficiently close together either the continuum assumption in the fluid breaks down or surface roughness of the particles become important. At this point the force experienced by the sphere can no longer be adequately described by the Navier–Stokes equation. Without this breakdown of lubrication, the energy associated with the relative motion of the particles would be dissipated before the particles could collide and rebound and hence collisions would never occur. However, the dependence of the suspension properties on the details of the lubrication breakdown is weak (Sangani *et al.* 1996) and so the exact details of the breakdown mechanism are of relatively little importance in the current context. The way that we treat this lubrication breakdown in the numerical simulations will be discussed in the following section.

Throughout this study we confine our attention to the case where the stresses exerted by the fluid on the particles are sufficiently small that they have a weak effect on the particle motions. Specifically, we will require that the particles have a velocity distribution close to a Maxwellian. If collisions are sufficiently close to being elastic, a Maxwellian velocity distribution is established in a hard-sphere suspension through the randomizing effects of collisions between particles. Therefore we will require that the time between collisions is much less than the time taken by the fluid forces to significantly affect the particle motion.

The mean time between successive interparticle collisions among hard spheres is (Chapman & Cowling 1970)

$$t_{coll} = \frac{a}{12\phi\chi}\sqrt{\frac{\pi}{T}}, \tag{10}$$

where χ is the value of the radial distribution function for a hard-sphere distribution at interparticle contact. The radial distribution function can be approximated by (Carnahan & Starling 1969)

$$\chi = \frac{1-\phi/2}{(1-\phi)^3}, \tag{11}$$

for $\phi < 0.5$ and by an empirical function given by Ma & Ahmadi (1988) for larger values of ϕ.

The time required for the fluid stresses to significantly affect the particle motion is given by the ratio of the typical particle momentum to the typical force, F, experienced by a particle, that is

$$t_{fluid} = \frac{m\sqrt{3T}}{F}. \tag{12}$$

Our theory will require that

$$W \equiv \frac{t_{fluid}}{t_{coll}} = 12\sqrt{\frac{3}{\pi}}\phi\chi\frac{mT}{Fa} \gg 1. \tag{13}$$

A priori it is unclear what the scaling for the force, F, will be. For example, an isolated sphere in a mean flow feels a force that depends on the Reynolds number in a complicated way (Clift, Grace & Weber 1978). So we must determine the scaling

and then *a posteri* ensure that the above condition is met. For dilute suspensions with low Reynolds number the force is given by the Stokes drag force, $F = 6\pi\mu a\sqrt{3T}$, and the condition reduces to

$$W = \frac{12\phi\chi}{\sqrt{\pi}} St \gg 1. \tag{14}$$

Continuum equations for mass, momentum and energy conservation together with the corresponding constitutive equations can be derived using standard techniques from statistical mechanics and kinetic theory. If the density ratio, ρ_p/ρ_f, is large the form of the equations is the same as those derived for gas–solid suspensions (Sangani *et al.* 1996; Koch & Sangani 1999), and similar to the equations for granular flow (Lun *et al.* 1984). However, if the density ratio is not large we must also take into account the kinetic energy contained in the fluid phase. The isotropic kinetic energy contained in the fluid phase can be determined from the isotropic Reynolds stress that is induced by the particle motion. Hence the total internal energy density, E, is given by

$$E = \tfrac{3}{2}\phi\rho_p T + \tfrac{1}{2}(1-\phi)\rho_f \langle \boldsymbol{u}' \cdot \boldsymbol{u}' \rangle_f, \tag{15}$$

where $\langle\cdot\rangle_f$ denotes the average over the volume occupied by the fluid phase and $\boldsymbol{u}' = \boldsymbol{u} - \langle \boldsymbol{U} \rangle$ is the deviation of the fluid velocity from the the mean particle velocity.

For nearly elastic collisions and weak viscous dissipation, i.e. $W \gg 1$, the energy balance is given by

$$\frac{\partial E}{\partial t} + \langle \boldsymbol{U} \rangle \cdot \nabla E = -\frac{\partial q_i}{\partial x_i} + \gamma_{ij}\sigma_{ij} - \Gamma, \tag{16}$$

where σ_{ij} is the bulk stress, γ_{ij} is the rate-of-strain tensor for the particle phase, q_i is the flux of fluctuation energy and Γ is the rate of energy dissipation per unit volume of the suspension. Since they are only weakly affected by the fluid stresses, the motion of the particles will be close to that of a dense gas with a hard-sphere interaction potential.

The total energy dissipation is the sum of two components; the first arises from the inelastic collisions between particles and the second is due to viscous stresses exerted on the particles by the fluid.

The dissipation due to inelastic effects is given by

$$\Gamma_{inelas} = \frac{12}{a\pi^{1/2}}(1-e)\rho_p\phi^2\chi T^{3/2}, \tag{17}$$

where e is the coefficient of restitution for particle collisions.

The rate of viscous energy dissipation in a suspension with zero mean relative motion between the particles and the fluid phases can be expressed as

$$\Gamma_{vis} = -n\langle \boldsymbol{F} \cdot (\boldsymbol{U} - \langle \boldsymbol{U} \rangle) + (\Omega - \langle \Omega \rangle) \cdot \mathscr{L} \rangle = 18\pi\mu a n T R_{diss}(Re_T, \phi, \epsilon_m). \tag{18}$$

The dissipation coefficient, R_{diss} can be interpreted as an effective drag coefficient. It is a function of the fluctuation Reynolds number, Re_T, the volume fraction, ϕ, and the way in which the lubrication flow breaks down that is described by the parameter, ϵ_m (see § 3).

The relative importance of inelastic and viscous dissipation can be measured in terms of

$$\frac{\Gamma_{inelas}}{\Gamma_{vis}} = \frac{\rho_p}{\rho_f}\frac{4(1-e)\phi\chi Re_T}{9\pi^{1/2}R_{diss}}. \tag{19}$$

Despite the assumption that $W \gg 1$, the ratio can still be small so that viscous dissipation dominates over collisional dissipation. In this paper we will consider the case in which the dissipation due to inelasticity is negligible compared to the dissipation due to viscous forces, and will show later that this is the case for a wide range of important physical parameters.

To treat suspensions with larger deviations from isotropy, i.e. lower values of W, one can adopt the procedure developed by Sangani *et al.* (1996) and solve an equation for the second-moment tensor of the fluctuating velocity field. They showed for low-Reynolds-number suspensions that including a term $18\pi\mu an T_{ij} R_{diss}$ in the equation for $T_{ij} = \langle (U_i - \langle U_i \rangle)(U_j - \langle U_j \rangle) \rangle$ yielded a moment equation whose predictions were in accord with dynamic simulations for simple shear flow at moderate W.

When particles translate through the suspension they transport their own momentum ($m\boldsymbol{U}$) giving rise to the particle kinetic contributions to the suspension stress. However, the particles induce fluctuating velocities in the fluid which also transport momentum. In addition, when particles collide the momentum transport includes an instantaneous change in the velocity of the fluid as well as instantaneous changes in particle velocity. For a potential flow, a detailed theory (Kang *et al.* 1997) has been developed using the fact that the fluid responds instantaneously to collisional changes in the velocity of the particle (or bubble). Their results require the standard expressions for the kinetic and collisional stress and flux of fluctuating energy to be multiplied by the factor

$$\left[1 + \frac{(1-\phi)}{\phi} \frac{\rho_f}{\rho_p} \frac{\langle \boldsymbol{u}' \cdot \boldsymbol{u}' \rangle_f}{3T}\right], \tag{20}$$

which takes into account the mass of the surrounding fluid that the particle must accelerate (added mass). For a moderate-Reynolds-number viscous flow, the situation is more complicated since the fluid flow will not change instantaneously upon interparticle collision. However, one can argue that ultimately the particle must also accelerate the surrounding fluid and the time lag is of limited importance to the magnitude of the bulk stress. Therefore we will adopt the expressions derived for potential flow until a more sophisticated theory is available.

3. Numerical method

In order to progress with the above problem we solve the Navier–Stokes equations in the fluid phase using a lattice-Boltzmann (LB) technique. The LB algorithm provides a flexible and accurate method for solving the Navier–Stokes equation in complex domains. A full description of the method can be found in Ladd (1994*a*) and the accuracy and its importance to suspension mechanics is thoroughly discussed in Ladd (1994*b*). Hill *et al.* (2001*a*, *b*) provide a detailed discussion of the grid resolution required to accurately simulate flow through fixed beds over a wide range of particle volume fractions and Reynolds numbers. The resolution used in this study was similar.

We consider the limit of high particle inertia so that the particle velocities are only weakly affected by the hydrodynamic forces between successive interparticle collisions. The collisions are treated as perfectly elastic. Thus, the velocity distribution of the particles is expected to be nearly Maxwellian and the particle positions take on a hard-sphere distribution. The particle positions and velocities are chosen initially from hard-sphere and Maxwellian distributions and are advanced using a hard-sphere

algorithm. The hydrodynamic forces exerted on the particles are used to compute the average dissipation of fluctuating kinetic energy and the average drag force.

An unbounded suspension is approximated by a suspension containing many particles in a cubic unit cell with periodic boundary conditions. We use a box size that is sufficiently large so that further increases in box size have a negligible (typically less than 1%) effect on the mean dissipation. We have ensured that the box sizes are large enough that particle correlations across the box size are negligible (appropriate for dense suspensions) and that the fluid correlations (appropriate for dilute suspensions), which decay over the Brinkman screening length (Hinch 1977) are also negligible. It was typically found that choosing the periodic box size such that it contained between 30 and 40 spheres gave accurate results.

If continuum lubrication forces between smooth spherical particles applied at all interparticle separations, then the singular nature of the lubrication interaction would arrest the relative motion of the colliding particles preventing particles from bouncing. However, for high-Stokes-number particles, any particle roughness or non-continuum fluid behaviour that occurs at small separations will allow particles to bounce. The dependence of the viscous dissipation on the exact nature of this breakdown mechanism is weak (Sangani *et al.* 1996).

Sangani *et al.* define the parameter ϵ_m which corresponds to the non-dimensional gap thickness at which the lubrication force stops following the continuum form and becomes a constant. If the profile of the lubrication force as a function of gap thickness is different from this assumed form then one can obtain an equivalent ϵ_m that gives the same viscous dissipation during a lubrication collision. This was illustrated by Sangani *et al.* for the case of lubrication breakdown due to the finite mean free path of the suspending gas.

In our simulations, lubrication breaks down as a result of the finite resolution of the grid. This is illustrated in figure 1 where we compare the results of a low-Reynolds-number LB simulation and a Stokes flow calculation using a modified-multipole method (Sangani *et al.* 1996) in calculating the force caused by relative motion of two particles along their line-of-centres. The LB method is in good agreement with the modified-multipole calculation for separations significantly smaller than one grid spacing. However, at very small separations, the LB calculation yields a finite force whereas the actual lubrication force diverges. Because different ratios of the particle radius to the grid spacing were used for calculations at different Reynolds numbers and volume fractions, the ratio ϵ_m varied in our computations. However, provided that $\epsilon_m \ll 1/Re_T$, the particle interactions are dominated by viscous forces at separations comparable with ϵ_m. This observation provides a means of adjusting our results to a constant value of ϵ_m. For a given grid resolution, computations for $Re_T \ll 1$ were compared with the results of the modified-multipole method and the value of ϵ_m was chosen to yield the same viscous dissipation of energy as for a two-particle collision. This ϵ_m was then used for comparisons at all Re_T and ϕ. For consistency, the results of calculations with different grid resolutions were then adjusted to a single value $\epsilon_m = 0.003$ by using equation (21) below and noting that the collisional-lubrication contribution to the dissipation is independent of Re_T.

The LB method solves the Navier–Stokes equations within the entire fluid volume. Therefore simulations at very low volume fractions tend to be computationally expensive because of the large number of points required to make the box length much larger than the Brinkman screening length. This has the unfortunate consequence of making comparison of simulation results with dilute theories computationally impractical.

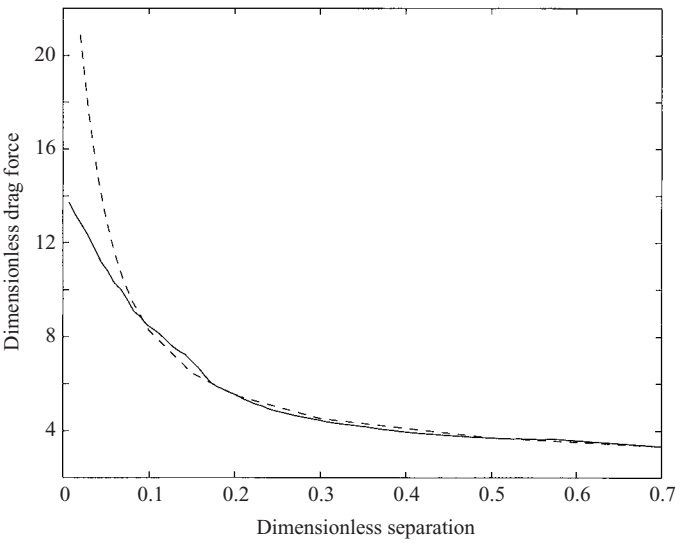

FIGURE 1. Two spheres collide along their line of centres with velocity U in a periodic box whose length is approximately 7 times the particle radius. The drag force on each sphere is calculated and made dimensionless by dividing by $6\pi\mu aU$ and the separation is made dimensionless by dividing by the particle radius. The solid line shows the result of the LB method using a particle of diameter nine grid spaces. The dashed line shows the result for a high-accuracy modified-multipole calculation. The agreement is good even when the separation is considerably less than one grid spacing (a dimensionless separation of 0.22 in this case). The data are used to calculate the effective lubrication cutoff when calculating the dissipation in the simulations. For different grid resolutions of the particles, different values of the lubrication cutoff are obtained, but the dissipation can be trivially modified using equation (21) so that the results are consistent (see discussion in § 3).

4. Viscous dissipation in the absence of a mean relative motion

4.1. *Simulation results*

At $Re_T = 0$ the rate of dissipation has been calculated by Sangani *et al.* (1996). They used a modified-multipole method to simulate Stokes flow in the fluid phase and obtained the result

$$R_{diss0} \equiv R_{diss}(0, \phi, \epsilon_m) = k_1(\phi) - k_2(\phi) \ln \epsilon_m, \tag{21}$$

where

$$k_1(\phi) = 1 + 3\sqrt{\frac{\phi}{2}} + \frac{135}{64}\phi \ln \phi + 11.26\phi(1 - 5.1\phi + 16.57\phi^2 - 21.77\phi^3), \tag{22}$$

and

$$k_2(\phi) = \phi\chi. \tag{23}$$

By considering simulations at low Reynolds number we can extrapolate and compare our calculations with the $Re_T = 0$ results of Sangani *et al.* (1996). The comparison is shown in figure 2. At low Re_T, a simple asymptotic expansion (Koch & Ladd 1997) shows that the $O(Re_T)$ contributions to the conditionally averaged velocity and pressure fields with one particle position specified must be odd and even functions of

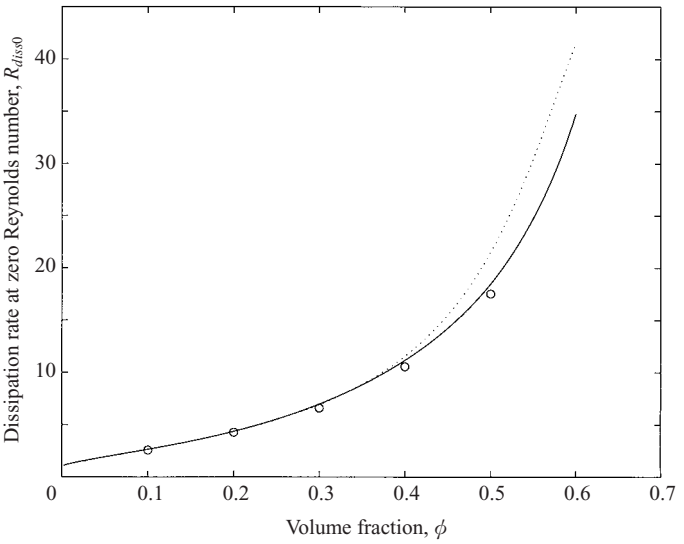

FIGURE 2. The dimensionless dissipation coefficient at zero Reynolds number, R_{diss0}, is plotted against the volume fraction. The circles represent results from the LB simulations, the solid line represents the results obtained by Sangani *et al.* using a modified-multipole method and the dotted line is the result of a theory developed using results from fixed beds. The theory and simulations are in excellent agreement up to volume fractions of approximately 0.4 and reasonable right up to close packing.

position relative to the test particle, respectively. Hence the first effects of inertia on the dissipation appear at order Re_T^2:

$$R_{diss}(Re_T, \phi, \epsilon_m) = R_{diss0} + Re_T^2 C(\phi) \qquad \text{as} \qquad Re_T \to 0. \tag{24}$$

The coefficient C, which is shown in figure 3, is independent of ϵ_m because inertia is negligible when the particles are as close as the lubrication cutoff. The quadratic behaviour of the dissipation with Reynolds number is confined to the region $Re_T < 1$ and thus this quadratic region is of rather limited interest.

Results for larger Reynolds number are shown in figure 4. They indicate that R_{diss} increases linearly with Reynolds number for $Re_T > 1$. In a similar manner Hill *et al.* (2001*b*) found that the drag coefficient for pressure-driven flow through a fixed bed of particles is a linear function of the Reynolds number based on mean velocity for sufficiently large Reynolds numbers. We find that at large Re, a good approximation is given by

$$R_{diss}(Re_T, \phi, \epsilon_m) = R_{diss0} + Re_T K(\phi). \tag{25}$$

The coefficient K is shown in figure 5. In fact, the large-Re_T results are slightly smaller than the approximation because of the quadratic behaviour for small Re_T. However, this formula is accurate to within approximately 4% over the entire range of Reynolds numbers considered in this study. Due to its accuracy and simplicity we choose to use this formula to describe the whole range of Reynolds numbers. This linear scaling at large Re_T is by no means obvious, but it is interesting to compare this result with experiments in densely packed fixed beds by Ergun (1952) who also observed a linear

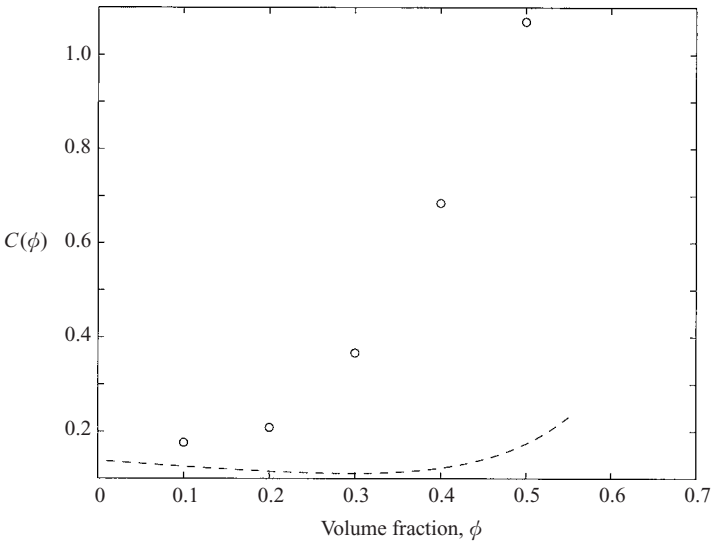

FIGURE 3. The coefficient C in equation (24), which represents the first effects of fluid inertia on the dissipation, is plotted against the volume fraction. The circles show results of LB simulations and the dashed line is a theory developed using results from fixed beds. The comparison is quite poor except at low volume fractions.

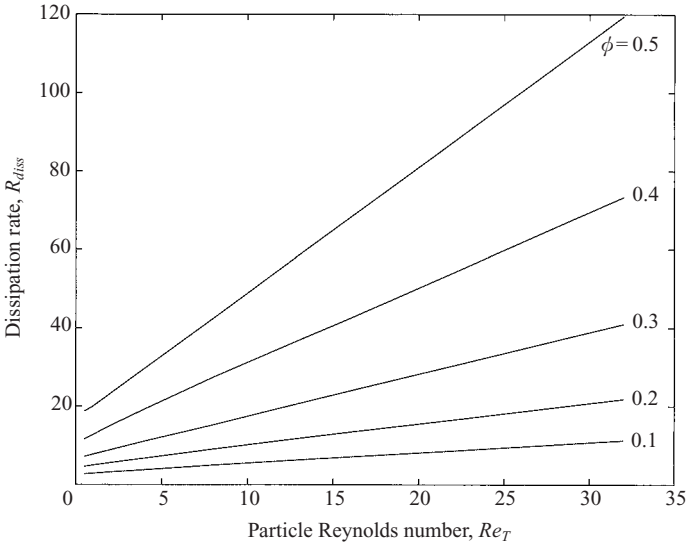

FIGURE 4. The dimensionless dissipation coefficient, R_{diss}, is plotted against the Reynolds number, Re_T, for a range of volume fractions. At large Re_T the dissipation rate is found to increase linearly with Re_T.

increase at large Re. An estimate of K, that also fits a low-volume-fraction theory developed in the next section to leading order, is given by

$$K(\phi) = \frac{0.096 + 0.142\phi^{0.212}}{(1-\phi)^{4.454}}. \tag{26}$$

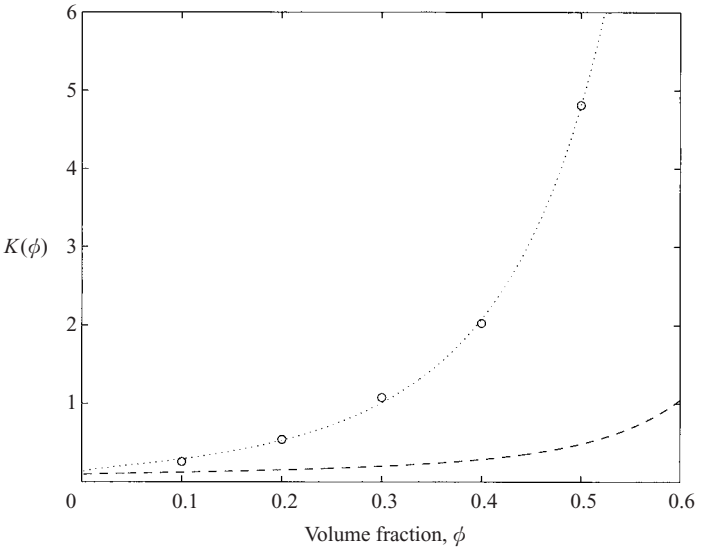

FIGURE 5. The coefficient K in equation (25), which represents the effects of significant fluid inertia on the dissipation rate, is plotted against the volume fraction. The circles represent results from the LB simulations, the dashed line is the result of a theory developed using results from fixed beds and the dotted line is a fit to the LB data. The comparison between results and theory is quite poor except at low volume fractions.

We are now in a position to examine in detail the assumptions made in formulating the theory. The characteristic magnitude of the force experienced by a particle is given by

$$\langle F^2 \rangle^{1/2} = 6\pi\mu a\sqrt{3T}\,R_{diss}. \tag{27}$$

For large values of the Reynolds number this scales as

$$F \sim \rho_f a^2 T, \tag{28}$$

which is the scale for the inertial Reynolds stress for a moving particle. The condition that the suspension has an isotropic Maxwellian distribution of particle velocities is given by

$$W = \frac{4\phi\chi}{3\sqrt{\pi}}\frac{\rho_p}{\rho_f}\frac{Re_T}{R_{diss0} + K\,Re_T} \gg 1. \tag{29}$$

The data from the low-Reynolds-number simulations of Wylie & Koch (2000) show that the dissipation can be accurately estimated by the theory for $W > 2$. For lower values of W, particle clustering occurs because the viscous drag felt by a particle is larger when it is in the vicinity of other particles. This enhanced drag means that particles dissipate more of their kinetic energy in the presence of neighbours and so are more likely to aggregate. For larger Reynolds numbers the force felt by the particle will be dominated by the contribution due to the form drag rather than the viscous stress. The form drag will not increase as strongly as the viscous stress when the particle is in the vicinity of other particles. Hence we expect that the above condition may be a more conservative bound in the case of large Reynolds number. However, we should also note that although the suspension should be more isotropic at high Re the nonlinear form of the drag law may affect the velocity distribution for

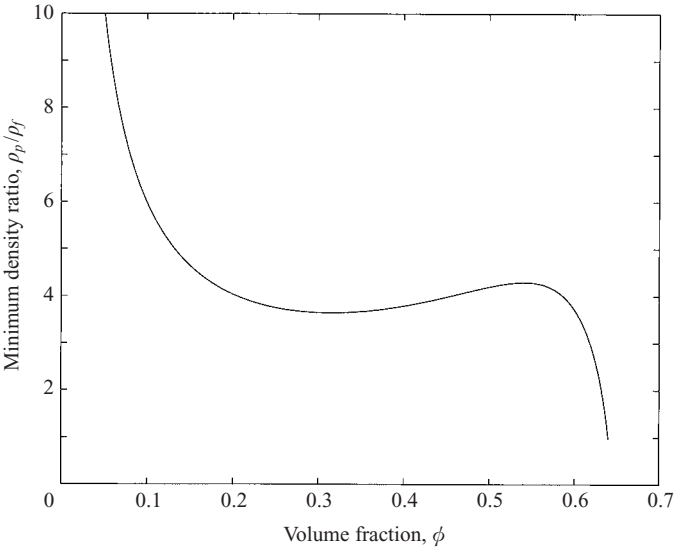

FIGURE 6. A conservative estimate of the minimum ratio of the particle density to fluid density required for the assumption of Maxwellian-distributed particle velocities to be valid is plotted against volume fraction.

the faster moving particles (as seen in the analysis for dilute sheared suspensions by Tsao & Koch 1995) and this may lead to significant discrepancies.

After some trivial rearrangement, the condition that the particle velocity distribution remains isotropic and Maxwellian is given by

$$Re_T \left(\frac{2\phi\chi}{3\sqrt{\pi}} \frac{\rho_p}{\rho_f} - K \right) > R_{diss0}. \tag{30}$$

A necessary condition for this to be true is

$$\frac{\rho_p}{\rho_f} > \frac{3\sqrt{\pi}K}{2\phi\chi}. \tag{31}$$

This condition is plotted in figure 6. It turns out to be slightly restrictive for very low values of the volume fraction, so that only gas–solid suspensions can be considered, but for moderate to high values of the volume fraction it will be generally satisfied for the majority of metal or other dense materials in water. In fact, as noted above, the restriction may be rather conservative at higher values of the Reynolds number and so the theory will also probably be applicable to environmental slurry and sedimentary flows in which rock or silica-based material is suspended in water.

For our results to be of interest we also require that viscous dissipation is larger than dissipation due to inelastic collisions. The ratio is given by

$$\frac{\Gamma_{inelas}}{\Gamma_{vis}} = \frac{\rho_p}{\rho_f} \frac{4(1-e)\phi\chi\, Re_T}{9\pi^{1/2}(R_{diss0} + K\, Re_T)}. \tag{32}$$

So for viscous dissipation to dominate we require

$$Re_T \left(\frac{\rho_p}{\rho_f} \frac{4(1-e)\phi\chi}{9\pi^{1/2}} - K \right) < R_{diss0}. \tag{33}$$

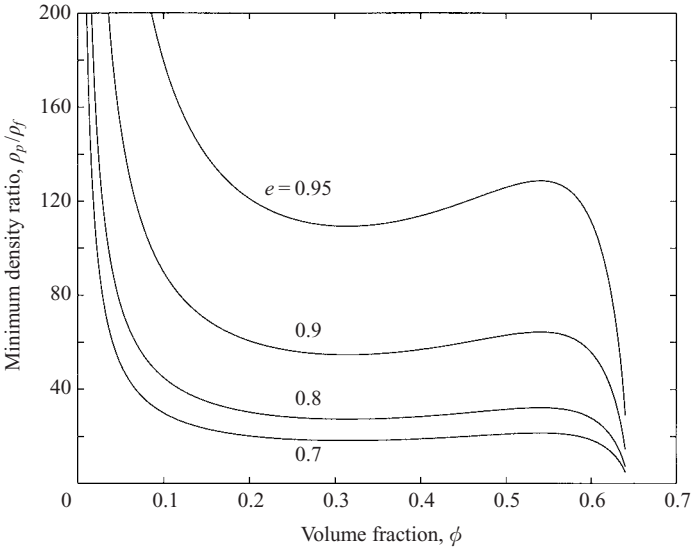

FIGURE 7. A sufficient condition to ensure that the dissipation due to fluid stresses is greater than the dissipation due to inelasticity in collisions requires that the ratio of the particle density to the fluid density is less than the plotted value. The value is plotted against volume fraction and for a range of coefficients of elasticity, e.

This will always be satisfied when

$$\frac{\rho_p}{\rho_f} < \frac{9\pi^{1/2}K}{4(1-e)\phi\chi}. \tag{34}$$

This density condition is plotted in figure 7 for various values of the coefficient of restitution e. This condition is easily satisfied for a wide range of suspensions and will only fail in gas–solid suspensions when the volume fraction is sufficiently large. Even when the density condition fails, the viscous dissipation can still be dominant as long as the Reynolds number is not too large compared to R_{diss0}/K.

In order to determine the amount of energy in the fluid phase we must also consider the velocity variance (Reynolds stress) of the fluid as a function of Re_T. It is clear that at low volume fractions this energy will be significant when compared with the energy contained in the solid phase if the density ratio ρ_p/ρ_f is not too large. For the isotropic suspensions simulated here, the fluid velocity variance characterizes the magnitude of the isotropic Reynolds stress in the fluid produced by the random particle motions. The variance as a function of Reynolds number is shown in figure 8 for volume fractions $\phi = 0.1$, 0.2, 0.3, 0.4 and 0.5. It is characterized by an initial decrease from its value at $Re_T = 0$ followed by an increase as Re_T is increased further.

At small Re_T and small ϕ, the variance is large and is limited only by the Brinkman screening due to particle–particle interactions. However, as Re_T is increased, the fluid inertia becomes important at distances from a particle that are smaller than the Brinkman screening length. This leads to a decrease in the velocity variance at small Re_T. Kaneda's (1986) solution for the velocity disturbance in a finite-Reynolds-number fixed bed illustrates this effect. At sufficiently larger Reynolds numbers, the time required for the vorticity shed by each particle to diffuse and dissipate becomes longer and so the fluid velocity variance increases. At larger volume fractions the initial decrease in the fluid velocity variance with increasing Re_T becomes weaker

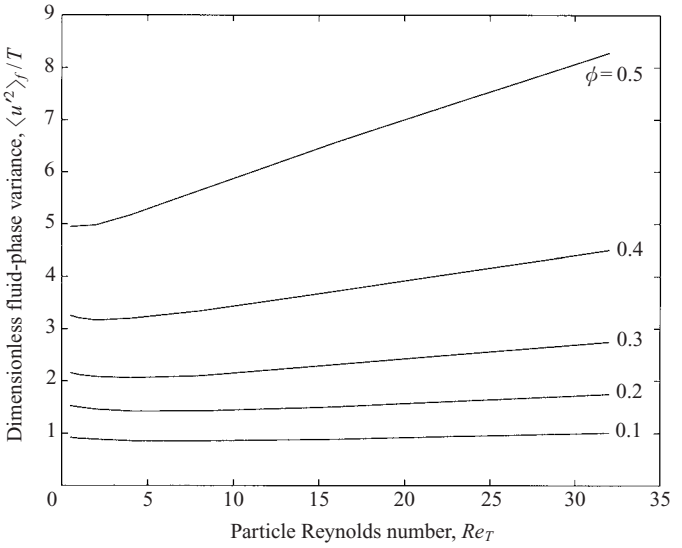

FIGURE 8. The fluid-phase variance divided by the granular temperature is plotted against the Reynolds number Re_T for a range of volume fractions.

because particle interactions screen the velocity disturbances at small length scales so that inertia plays less of a role.

4.2. *A simple theory for* R_{diss}

The hydrodynamic interactions among the particles in a large-W suspension are similar to those in a fixed bed. The large inertia of the particles implies that a particle's velocity is relatively unresponsive to the hydrodynamic force acting on the particle. Thus, in each case, the fluid motion induced by a test particle produces hydrodynamic forces acting on the surrounding particles that are opposite to the hydrodynamic force on the test particle and tend to screen its hydrodynamic disturbance. In a low-Reynolds-number suspension, this phenomenon is referred to as Brinkman screening. Thus, we might choose to approximate the drag on a particle moving through a finite-Re_T, large-W suspension by the drag on a single moving particle in a fixed bed. The force on a fixed particle in a fixed bed subject to a pressure-driven flow has been calculated by Hill *et al.* (2001*b*) and is given by

$$\boldsymbol{F} = 6\pi\mu a R_d(Re_T, \phi)\boldsymbol{U}_m, \tag{35}$$

where R_d is the drag coefficient and $\boldsymbol{U}_m$ is the mean fluid velocity. At zero Reynolds number it can be approximated by (Koch & Sangani 1999)

$$R_{d0} \equiv R_d(0, \phi) = \frac{1 + 3/\sqrt{2}\phi^{1/2} + (135/64)\phi \ln \phi + 17.14\phi}{1 + 0.681\phi - 8.48\phi^2 + 8.16\phi^3}. \tag{36}$$

In the suspension, there is no net pressure gradient and so we must subtract the component of the drag that arises from the mean pressure gradient. This is explicitly known since this component of the drag must balance the drag on a sphere multiplied by the number of spheres per unit volume. Hence the force on the test particle, $\boldsymbol{F}_p$, is given by

$$\boldsymbol{F}_p = 6\pi\mu a(1 - \phi)R_d\boldsymbol{U}_p, \tag{37}$$

where $\boldsymbol{U}_p$ is the velocity of the test particle.

To use this result to estimate R_{diss}, we must now calculate the energy dissipation for the sphere's motion and then take into account the range of possible velocities of the test particle by integrating over the Maxwellian. The rate of dissipation of energy by the particle motion is given by

$$\boldsymbol{F}_p \cdot \boldsymbol{U}_p = 6\pi\mu a R_d U_p^2. \tag{38}$$

Integrating over the Maxwellian distribution (taking careful account of the fact that Re_T contains velocity-dependent terms) then gives the total rate of energy dissipation.

In a fixed bed, the particle velocities are all zero whereas in the suspension considered here they take a Maxwellian velocity distribution in the sense that the fluid velocity disturbance produced by one particle has a weak effect on the motion of neighbouring particles. We have partially corrected for this difference by removing the average pressure gradient driving the liquid flow in a fixed bed. In a low-Reynolds-number suspension, this results in an approximation that describes correctly the long-range hydrodynamic interactions associated with the net forces acting on the particles. However, the higher-order multipoles and lubrication interactions among the moving particles will be different from those in the fixed bed. Therefore, we expect this simple approximation to be most accurate at small volume fractions. The deviations from the approximation give us an indication of the importance of relative motion of the particles.

At zero Reynolds number R_d is independent of $\boldsymbol{U}_p$ and the calculation becomes trivial. We obtain the simple result

$$R_{diss0} = (1-\phi)R_{d0}. \tag{39}$$

The comparison is shown in figure 2, with the value of the lubrication taken to be the reference value of 0.003 chosen by Sangani *et al.* (1997). The agreement between theory and simulations is remarkable up to volume fractions of $\phi = 0.4$ and good even up to near close packing. The agreement at very high volume fractions must be partly fortuitous because in this region lubrication interactions strongly affect R_{diss} but not R_d.

At low Reynolds number the results of Hill *et al.* (2001*a*) give the expression for drag as

$$R_d(\phi, Re_T) = R_{d0} + Re_T^2 C_{fb}(\phi), \tag{40}$$

where $C_{fb} = 0.0275 + \exp(11.6\phi - 8.97)$. After repeating the above procedure we find that

$$R_{diss} = (1-\phi)\left(R_{d0} + 5Re_T^2 C_{fb}\right) \qquad \text{as} \qquad Re_T \to 0. \tag{41}$$

At larger Reynolds numbers the drag can be approximated by

$$R_d(\phi, Re_T) = R_{d0} + Re_T K_{fb}(\phi), \tag{42}$$

where $K_{fb} = 0.0336 + 0.106\phi + 0.0116/(1-\phi)^5$. Repeating the above procedure gives

$$R_{diss} = (1-\phi)\left(R_{d0} + \frac{16K_{fb}}{3\sqrt{2\pi}} Re_T\right). \tag{43}$$

The theory and simulations can be compared in figures 3 and 5. Although the agreement is reasonable at low volume fractions, the overall agreement is poor especially at larger volume fractions.

We now discuss the relevance of the assumptions we made in developing the theory and carefully consider the results in this context. The theory, which assumes that the

dissipation is unaffected by motion of the particles surrounding the test particle, is seen to be in excellent agreement with simulations when fluid inertia is negligible. This is perhaps not very surprising for the following reason. The theory assumes that neighbours are stationary and neglects their motions. At zero Reynolds number neighbours moving in the same direction as the test particle will exert a smaller drag on the test particle than a corresponding stationary particle and particles moving in the opposite direction will exert a larger drag on the test particle than a corresponding stationary particle. Since the average velocity of the neighbours is zero and the total drag is linear in the velocity difference between the particle and its neighbours the drag on the test particle should be approximated well by assuming stationary neighbours. Thus, at zero Reynolds number, the simple model would be exact if all the interactions could be described in terms of a constant velocity near one particle caused by neighbouring particles.

Inertial effects at both low and high Re_T are described reasonably well by the theory at low volume fractions. However, the predictions of the theory for the inertial corrections at higher volume fractions are poor. This shows that for moderate to large volume fractions the fluid inertia due to the motions of the neighbours plays an important role in determining the additional dissipation due to inertia. This is not too surprising since the theory assumed that neighbours were stationary. At low volume fractions the fluid disturbances due to the motion of the neighbours will decay significantly before reaching the test particle and so the error incurred is not too large. At higher volume fractions the fluid motion produced by neighbours will have a significant effect on the drag. Because of the nonlinear nature of the drag force, close neighbours moving in the same direction as the test particle will have a much smaller effect on the drag than neighbours moving in the opposite direction. Therefore we should expect the rate of dissipation to be significantly higher than the theory. At low Reynolds number the inertial component of the drag scales like Re_T^2 whereas the large Reynolds numbers give a inertia component of the drag that scales like Re_T. The coefficient for the first effects of inertia (C) is more poorly estimated by the theory than the large-Re effects (measured by K) since the nonlinearity in the inertial correction to the drag force is stronger for low Reynolds numbers.

5. Results for dissipation and drag in the presence of a mean flow

5.1. *Simulation results*

Body forces will normally result in a mean relative motion between the particles and the fluid, in addition to any motion caused by shearing. Furthermore, fluidized beds exhibit random particle velocity fluctuations as well as a mean relative motion of the two phases. Kinetic theory formulations are often invoked to explain the continuum equations for fluidized beds (Koch & Sangani 1999; Sinclair & Jackson 1989; Gidaspow 1994; Pita & Sundaresan 1991). At low Re the treatment of such systems is simplified by the linearity of the Stokes equations so that the contributions from the mean flow and temperature are additive. However, at moderate Re, the nonlinearity in the Navier–Stokes equation will lead to significant coupling between the mean flow and temperature and we expect that this will have a significant effect on the dynamics of such systems.

To model such suspensions, we consider an array of particles with a Maxwellian distribution of velocities. The simulation procedure is the same as that used above, except that a constant body force density is exerted on the fluid to induce a mean

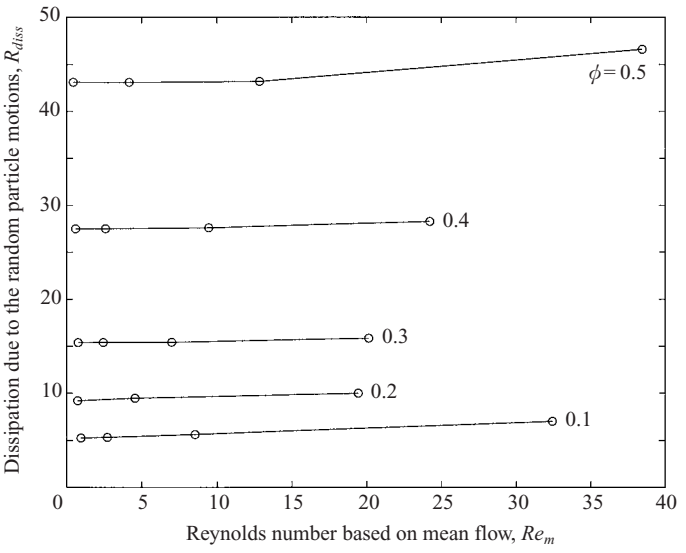

FIGURE 9. The dimensionless dissipation due to the random particle motions is plotted against the Reynolds number based on the mean flow, Re_m for various values of the volume fraction and a value of Reynolds number based on the granular temperature, $Re_T = 8$.

relative motion. The mean velocity of the fluid is computed and the mean drag on the particles is equal to the specified body force.

We define the drag coefficient, R_d, as for fixed beds:

$$R_d = \frac{\langle \boldsymbol{F} \rangle \cdot \boldsymbol{U}_m}{6\pi\mu a U_m^2}, \tag{44}$$

where $\boldsymbol{U}_m$ is the the mean flow velocity and $\boldsymbol{F}$ is the force experienced by an individual particle. The Reynolds number based on the mean flow is given by

$$Re_m = \frac{2\rho_f a|\boldsymbol{U}_m|}{\mu}. \tag{45}$$

The total dissipation has a component that arises from the mean flow. We therefore define R_{diss} to be the dimensionless rate of dissipation that occurs due to the granular temperature,

$$R_{diss} = \frac{\langle \boldsymbol{F} \cdot (\boldsymbol{U} - U_m) \rangle}{18\pi\mu a T}, \tag{46}$$

where $\boldsymbol{U}$ is the velocity of an individual particle. It is clear that this quantity will be affected by the mean flow, but it represents the increase due to nonlinear coupling.

Due to the larger parameter space and the computationally expensive nature of these simulations, a full determination for the entire range of parameters was not possible. We therefore considered a wide range of values for Re_T and Re_m at a single volume fraction ($\phi = 0.2$), and then considered the variation of the results with Re_m for additional values of the volume fraction. In the next section we will present a theory that allows a reasonably accurate prediction of the simulation results for R_d.

Figures 9 and 10 show the variation of R_{diss} and R_d with mean flow for various volume fractions and a constant value of $Re_T = 8$. The percentage change in R_d due

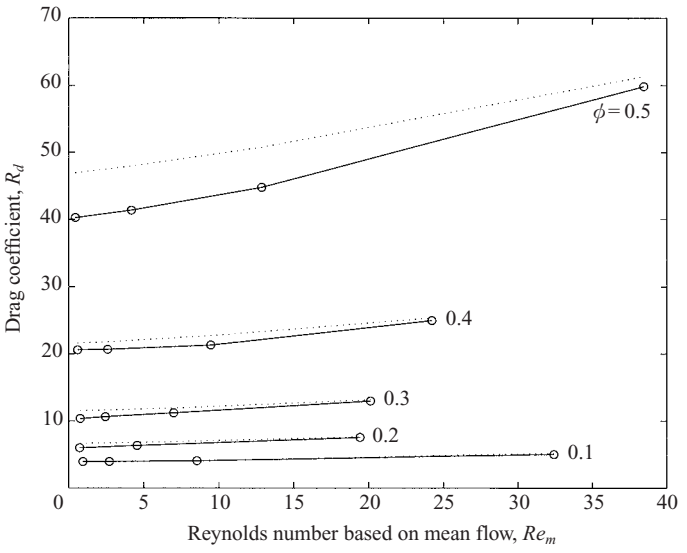

FIGURE 10. The dimensionless drag is plotted against the Reynolds number based on the mean flow, Re_m for various values of the volume fraction and $Re_T = 8$. The circles represent the results from LB simulations and the dotted lines represent the results of a theory based on results obtained from fixed beds.

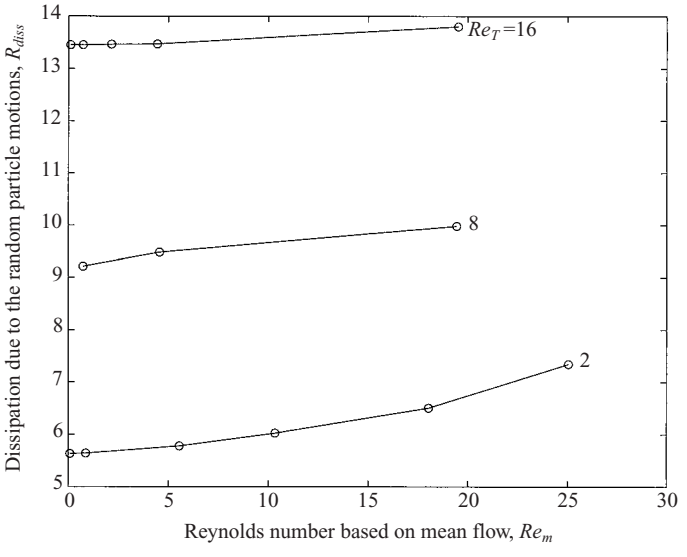

FIGURE 11. The dimensionless dissipation due to the random particle motions is plotted against the Reynolds number based on the mean flow, Re_m for various values of the Reynolds number based on the granular temperature, Re_T at a volume fraction of $\phi = 0.2$.

to the mean flow is typically greater than three times the percentage change in R_{diss}. Also, the variation in R_{diss} is very small when $Re_m < Re_T$.

Figures 11 and 12 show the variation of R_{diss} and R_d with mean flow for various values of Re_T and a constant value of the volume fraction $\phi = 0.2$. Again, the simulations show that R_{diss} is relatively insensitive to the mean flow, except in the case

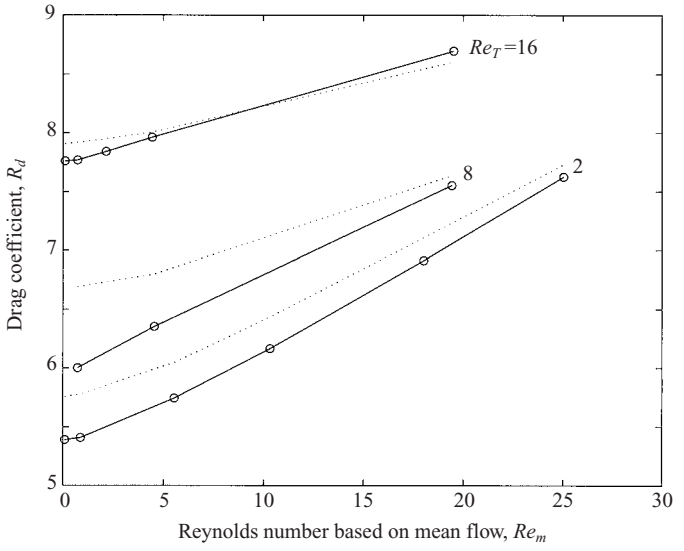

FIGURE 12. The dimensionless drag is plotted against the Reynolds number based on the mean flow, Re_m for various values of the Reynolds number based on the granular temperature, Re_T, at a volume fraction of $\phi = 0.2$. The circles represent the results from LB simulations and the dotted lines represent the results of a theory based on results obtained from fixed beds.

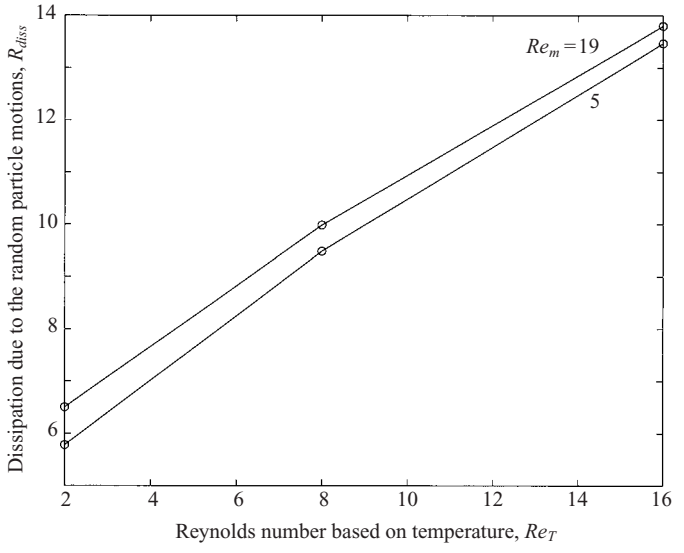

FIGURE 13. The dimensionless dissipation due to the random particle motions is plotted against the Reynolds number based on the granular temperature, Re_T, for two values of the Reynolds number based on the mean flow, Re_m, at volume fraction $\phi = 0.2$.

where Re_T is significantly larger than Re_m. This should be contratsed with R_d which varies significantly with the mean flow.

Figures 13 and 14 show the variation of R_{diss} and R_d with granular temperature for various values of Re_m and a constant value of the volume fraction $\phi = 0.2$. The sensitivity to Re_T seems to be considerably stronger than in the cases where Re_m varied, particularly the results for R_{diss}.

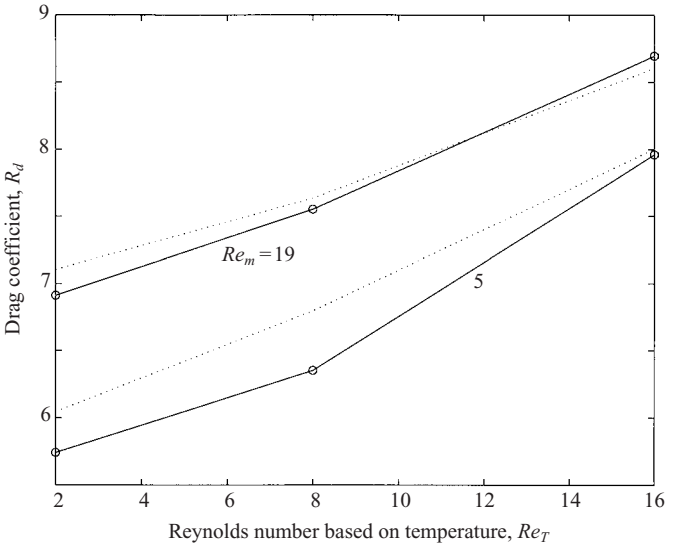

FIGURE 14. The dimensionless drag is plotted against the Reynolds number based on the granular temperature, Re_T, for two values of the Reynolds number based on the mean flow, Re_m, at volume fraction $\phi = 0.2$. The circles represent the results from LB simulations and the dotted lines represent the simple theory based on results obtained from fixed beds.

These results can be understood using the framework developed in § 4.2. The forces experienced by particles are nonlinear functions of both the random fluctuation velocity and the mean flow velocity. The forces that arise from the fluctuation velocities will take large values when two particles are moving rapidly in opposite directions, whereas the force due to mean flow cannot capture the nonlinearity as effectively. Hence the enhancement of the force due to Re_T will be greater than that due to Re_m except when Re_m is significantly larger than Re_T.

5.2. *A simple model for the mean drag force on particles with a Maxwellian velocity distribution*

In this section we develop an approximate theory that uses a similar approach to that used in our simple model for the dissipation rate in § 4.2. We again consider a test particle that is moving relative to its neighbours. As before, the neighbours are assumed to be fixed with respect to one another, but in this case the test particle experiences an additional drag force due to the mean flow of the gas. The velocity of the test particle relative to the gas, $\boldsymbol{U}_p$, consists of a mean flow $\boldsymbol{U}_m$ and a fluctuating velocity $\boldsymbol{U}_T$. Each particle in the suspension, stationary or moving, experiences a force $6\pi\mu a\phi R_d(Re_m)\boldsymbol{U}_m$ due to the mean pressure gradient required to drive the gas flow through the array of fixed particles. The additional force on the moving particle due to its motion with velocity $\boldsymbol{U}_p = \boldsymbol{U}_m + \boldsymbol{U}_T$ through a fixed bed is $6\pi\mu a(1-\phi)R_d(Re_p)\boldsymbol{U}_p$, so that the total force on the moving particle is

$$\boldsymbol{F} = 6\pi\mu a\phi R_d(Re_m)\boldsymbol{U}_m + 6\pi\mu a(1-\phi)R_d(Re_p)\boldsymbol{U}_p. \tag{47}$$

Then the drag coefficient for a given particle is given by

$$\frac{\boldsymbol{F}\cdot\boldsymbol{U}_m}{6\pi\mu a U_m^2} = \left[R_{d0} + \frac{2\rho_f K_{fb}}{\mu}\sqrt{U_m^2 + U_T^2 + 2|\boldsymbol{U}_m||\boldsymbol{U}_T|\cos\theta}\right]\left(1 + \frac{|\boldsymbol{U}_T|}{|\boldsymbol{U}_m|}\cos\theta\right), \tag{48}$$

where θ is the angle between $\boldsymbol{U}_T$ and $\boldsymbol{U}_m$. Averaging over the Maxwellian in $\boldsymbol{U}_T$ and taking care to correctly handle the branch cuts that occur when $|\boldsymbol{U}_T| = |\boldsymbol{U}_m|$, we obtain the result

$$R_d = R_{d0} + K_{fb} Re_m \left[\left(1 + \frac{2Re_T^2}{Re_m^2} - \frac{Re_T^4}{Re_m^4} \right) \operatorname{erf}\left(\frac{Re_m}{\sqrt{2} Re_T} \right) + \sqrt{\frac{2}{\pi}} \frac{Re_T}{Re_m} \left(1 + \frac{Re_T^2}{Re_m^2} \right) \exp\left(-\frac{Re_m^2}{2Re_T^2} \right) \right]. \quad (49)$$

The comparison between theory and simulations is shown in figures 10, 12 and 14. The agreement is generally good, with the largest errors around 10%. This shows which the relative motions of the neighbours, which made the agreement between the numerical results and the simple theory for the dissipation (§ 4.2) so poor, play a very weak role in modifying the drag coefficient. The accuracy of the theory for the drag coefficient increases when $Re_m > Re_T$ as one might expect.

It is also possible to develop a similar theory for the rate of dissipation. However, because the theory would not agree with the computations at zero mean flow if $Re_T = O(1)$ (see § 4) this theory would be of little practical use.

6. Discussion

We have calculated the rate of viscous dissipation of energy in a suspension with appreciable fluid inertia and large Stokes number, and presented a theory that allows for the coupled effects of mean and fluctuating motion of the particles with respect to the fluid. We now consider the consequences of this study for the rheology of suspensions and for the viscosity of a suspension under simple shear. In this case the granular temperature is generated by the external forcing and transmitted by interparticle collisions. This can be expressed in terms of the energy due to the shear work done by the particle viscosity. If $1 - e \ll 1$ and $W \gg 1$, so that the particle velocity distribution remains nearly isotropic and Maxwellian, this balance is given by

$$\frac{16}{5\sqrt{\pi}} \rho_p a T^{1/2} \phi^2 \chi J(\phi) \gamma^2 = \frac{27}{2a^2} \mu T \phi R_{diss}(Re_T, \phi, \epsilon_m) + \frac{12}{a\sqrt{\pi}} (1 - e) \rho_p \phi^2 \chi T^{3/2}, \quad (50)$$

where γ is the shear rate and

$$J(\phi) = 1 + \frac{\pi}{12} \left(1 + \frac{5}{8\phi\chi} \right)^2, \quad (51)$$

is calculated using kinetic theory (Lun *et al.* 1984).

We now compare the granular temperature and particle viscosity for three different regimes: elastic particles and low Re_T, elastic particles and high Re_T, and inelastic particles with negligible fluid effects. For low Re_T the dissipation is dominated by the viscous component and the granular temperature is given by

$$T = \frac{1024}{18225\pi} \frac{\phi^2 \chi^2 J^2}{R_{diss0}^2} \frac{\rho_p^2 a^6 \gamma^4}{\mu^2}, \quad (52)$$

and the particle viscosity is given by

$$\mu_p = \frac{512}{675\pi} \frac{\phi^3 \chi^2 J^2}{R_{diss0}} \frac{\rho_p^2 a^4 \gamma^2}{\mu}. \quad (53)$$

For large Re_T the dissipation is dominated by the form drag and the granular temperature is given by

$$T = \frac{16}{135\sqrt{\pi}} \frac{\phi \chi J}{K} \frac{\rho_p}{\rho_f} a^2 \gamma^2, \tag{54}$$

and the particle viscosity is given by

$$\mu_p = \left(\frac{4}{15\pi^{1/4}} \right)^3 \frac{\phi^{5/2} \chi^{3/2} J^{3/2}}{K^{1/2}} \sqrt{\frac{\rho_p}{\rho_f}} \rho_p a^2 \gamma. \tag{55}$$

If the effects of the fluid are negligible, the granular temperature is given by

$$T = \frac{4}{15} J \frac{a^2 \gamma^2}{(1-e)}, \tag{56}$$

and the particle viscosity is given by

$$\mu_p = \frac{32}{\sqrt{375\pi}} \phi^2 \chi J^{3/2} \frac{\rho_p a^2 \gamma}{(1-e)^{1/2}}. \tag{57}$$

If the dissipation is dominated by form drag (high Re_T) or by inelasticity (negligible fluid effects), the granular temperature and the particle viscosity have the same scalings with shear rate. This is because in each case the dissipation scales in the same way with granular temperature. In the case dominated by inelastic collisions the scaling for the dissipation is given by the amount of energy lost per collision ($\sim T$) multiplied by the collision rate ($\sim T^{1/2}$), whereas in the case dominated by Reynolds stress the scaling for the dissipation is given by the speed of the particle ($\sim T^{1/2}$) multiplied by the force experienced by the particle ($\sim T$).

This observation has the important consequence that it may be difficult to distinguish between the dissipative effects of inelasticity and inertial drag in experimental studies. Care must be taken when interpreting scalings of the mean shear stress and normal stress (which is proportional to T) with the shear rate and particle radius. One might easily obtain what appears to be the correct scaling for granular materials and conclude that fluid effects are negligible even though fluid effects give rise to the same scaling. One way of distinguishing the effects of dissipation due to form drag and inelasticity would be to vary the density ratio of the particles and fluid.

On the other hand, experimentalists may be able to make use of the similarity in the following way. Small-scale laboratory experiments on granular materials are notoriously difficult for a number of reasons, including difficulties in finding almost perfectly elastic particles, complicated boundary conditions, difficulties in achieving low or even moderate volume fractions and problems in overcoming frictional effects. But these results allow one to create a material that has the same dissipation rate and temperature by using a high-Reynolds-number suspension. The effective coefficient of restitution is simply given by

$$e_{eff} = e - \frac{9\sqrt{\pi} K}{4\phi\chi} \frac{\rho_f}{\rho_p}. \tag{58}$$

While these experiments are far from trivial, they eliminate many of the problems encountered and give a much wider range of possibilities.

The results for dissipation and drag in the presence of a mean relative motion of the phases have important implications for fluidized beds and pneumatic transport of materials. Koch (1990) and Koch & Sangani (1999) showed that the granular temperature in a high-Stokes-number sedimenting suspension occurs due to hydrodynamic

interactions between particles. In the absence of shear, the Reynolds number based on the granular temperature would be much less than the Reynolds number based on the mean flow. However, hydrodynamic instabilities or pressure-driven flows in a pipe or channel will lead to shearing motions that enhance the granular temperature significantly. In the present study, it was shown that the mean drag on the particles increases strongly with Re_T and this could imply that particles in high-shear regions (such as may occur near the solid boundaries to flow, for example) are much more strongly retarded than those in low-shear regions.

Financial support was obtained from NASA grant NAG3-1853, CERG grant 9040650/9040751 and from the Schlumberger Foundation.

REFERENCES

Aidun, C. K., Lu, Y. & Ding, E. J. 1998 *J. Fluid Mech.* **373**, 287.
Bagnold, R. 1956 *Proc. R. Soc. Lond.* A **225**, 49.
Batchelor, G. K. 1970 *J. Fluid Mech.* **41**, 545.
Bunner, B. & Tryggvason, G. 1999 *Phys. Fluids* **11**, 1967.
Carnahan, N. F. & Starling, K. E. 1969 *J. Chem. Phys.* **51**, 635.
Chapman, S. & Cowling, T. G. 1970 *The Mathematical Theory of Non-Uniform Gases.* Cambridge University Press.
Clift, R., Grace, J. R. & Weber, M. E. 1978 *Bubbles, Drops and Particles.* Academic.
Drew, D. A. & Passman, S. L. 1999 *Theory of Multicomponent Fluids.* Applied Mathematical Sciences, vol. 135. Springer.
Ergun, S. 1952 *Chem. Engng Prog.* **48**, 89.
Gidaspow, D. 1994 *Multiphase Flow and Fluidization.* Academic.
Haines, D. M. & Inman, D. L. 1985 *J. Fluid Mech.* **150**, 357.
Hill, R. J., Koch, D. L. & Ladd, A. J. C. 2001*a* *J. Fluid Mech.* **448**, 213.
Hill, R. J., Koch, D. L. & Ladd, A. J. C. 2001*b* *J. Fluid Mech.* **448**, 243.
Hinch, E. J. 1977 *J. Fluid Mech.* **83**, 695.
Jenkins, J. T. & Richman, M. W. 1998 *J. Fluid Mech.* **192**, 313.
Kaneda, Y. 1986 *J. Fluid Mech.* **167**, 455.
Kang, S.-Y., Sangani, A. S., Tsao, H.-K. & Koch, D. L. 1997 *Phys. Fluids* **9**, 1540.
Koch, D. L. 1990 *Phys. Fluids* A **2**, 1711.
Koch, D. L. & Hill, R. J. 2001 *Annu. Rev. Fluid Mech.* **33**, 619.
Koch, D. L. & Ladd, A. J. C. 1997 *J. Fluid Mech.* **349**, 31.
Koch, D. L. & Sangani, A. S. 1999 *J. Fluid Mech.* **400**, 229.
Ladd, A. J. C. 1994*a* *J. Fluid Mech.* **271**, 285.
Ladd, A. J. C. 1994*b* *J. Fluid Mech.* **271**, 311.
Lun, C. K. K., Savage, S. B., Jeffrey, D. J. & Jenkins, J. T. 1984 *J. Fluid Mech.* **140**, 223.
Ma, D. & Ahmadi, G. 1988 *Powder Technol.* **56**, 191.
Pita, J. A. & Sundaresan, S. 1991 *AIChE J.* **37**, 1009.
Qi, D. 1999 *J. Fluid Mech.* **385**, 41.
Sangani, A. S., Mo, G., Tsao, H. K. & Koch, D. L. 1996 *J. Fluid Mech.* **313**, 309.
Sinclair, J. L. & Jackson, R. 1989 *AIChE J.* **35**, 1473.
Tsao, H. K. & Koch, D. L. 1995 *J. Fluid Mech.* **296**, 211.
Wylie, J. J. & Koch, D. L. 2000 *Phys. Fluids* **12**, 964.